

## Accepted Manuscript

SPH as nonlocal regularisation method: Solution for instabilities due to strain-softening

R. Vignjevic, N. Djordjevic, S. Gemkow, T. De Vuyst, J. Campbell

PII: S0045-7825(14)00135-2

DOI: <http://dx.doi.org/10.1016/j.cma.2014.04.010>

Reference: CMA 10224

To appear in: *Computer Methods in Applied Mechanics and Engineering*

Received date: 19 December 2013

Revised date: 10 April 2014

Accepted date: 20 April 2014

Please cite this article as: R. Vignjevic, N. Djordjevic, S. Gemkow, T. De Vuyst, J. Campbell, SPH as nonlocal regularisation method: Solution for instabilities due to strain-softening, *Computer Methods in Applied Mechanics and Engineering* (2014), <http://dx.doi.org/10.1016/j.cma.2014.04.010>

This is a PDF file of an unedited manuscript that has been accepted for publication. As a service to our customers we are providing this early version of the manuscript. The manuscript will undergo copyediting, typesetting, and review of the resulting proof before it is published in its final form. Please note that during the production process errors may be discovered which could affect the content, and all legal disclaimers that apply to the journal pertain.



## SPH as Nonlocal Regularisation Method: Solution for Instabilities due to Strain-Softening

Authors: R. Vignjevic<sup>a)\*</sup>, N. Djordjevic<sup>a)</sup>, S. Gemkow<sup>a)</sup>, T. De Vuyst<sup>a)</sup>, J. Campbell<sup>a)</sup>

<sup>a)</sup> Department of Applied Mechanics and Astronautics, School of Engineering, Cranfield University, Bedfordshire, MK43 0AL, UK

email: [v.rade@cranfield.ac.uk](mailto:v.rade@cranfield.ac.uk)

tel: +44 (0) 1234 758276

fax: +44 (0) 1234 758207

\* Corresponding Author

### Highlights of the findings:

- Strain-softening process in the FEM is localised in a single element and cannot propagate;
- FE results in presence of strain-softening are highly mesh sensitive;
- Localisation effects related to material strain-softening are not present with the SPH method;
- Size of the softening zone was defined by the smoothing length and was increasing with the increasing smoothing length;
- For a fixed smoothing length  $h$ , the strain softening was independent of the particle density;

# SPH as Nonlocal Regularisation Method: Solution for Instabilities due to Strain-Softening

Authors: R. Vignjevic<sup>a)\*</sup>, N. Djordjevic<sup>a)</sup>, S. Gemkow<sup>a)</sup>, T. De Vuyst<sup>a)</sup>, J. Campbell<sup>a)</sup>

<sup>a)</sup> Department of Applied Mechanics and Astronautics, School of Engineering, Cranfield University, Bedfordshire, MK43 0AL, UK

email: [v.rade@cranfield.ac.uk](mailto:v.rade@cranfield.ac.uk)

tel: +44 (0) 1234 758276 fax: +44 (0) 1234 758207

\* Corresponding Author

## Abstract

Within the framework of continuum damage mechanics (CDM), mechanical loading leads to material damage and consequent degradation of material properties. This can result in strain softening behaviour, which when implemented as a local model in the finite element (FE) method, leads to an ill posed boundary value problem, resulting in significant mesh sensitivity of the solution. It is well-known that the addition of a characteristic length scale to CDM models, a non-local approach, maintains the character of the governing equations. In this paper, the similarities between the Smooth Particle Hydrodynamic (SPH) method and non-local integral regularisation methods are discussed. A 1D dynamic strain softening problem is used as the test problem for a series of numerical experiments, to investigate the behaviour of SPH. An analytical solution for the test problem is derived, following the solution for a 1D stress state derived by Bažant and Belytschko in 1985. An equivalent SPH model of the problem is developed, using the stable Total-Lagrange form of the method, combined with a local bi-linear elastic-damage strength model. A series of numerical experiments, using both SPH and FE solvers, demonstrate that the width of the strain softening region is controlled by the element size in FE, but in SPH it is controlled by the smoothing length rather than the inter-particle distance, which is the analogous to the element size in the FE method. This investigation indicates that the SPH method is inherently non-local numerical method and suggests that the SPH smoothing length should be linked to the material characteristic length scale in solid mechanics simulations.

**Keywords:** Smoothed Particle Hydrodynamics, SPH, nonlocal regularisation, strain softening, instability, continuum damage, brittle materials

## 1 Introduction

1 Within the framework of local continuum damage mechanics (CDM), material behaviour under mechanical  
2 loading includes degeneration of material properties due to damage. Material behaviour is typically  
3 described by local models, which evaluate state and internal variables at a single location in a numerical  
4 model with, consequently, a limited ability to take into account the non-local effects occurring in a material  
5 including damage. Within the framework of local CDM, material dynamic strain softening due to damage  
6 leads to an ill-posed initial boundary value problem where the governing hyperbolic differential equations  
7 become elliptic, this leads to instability of the continuum solution with an infinite number of bifurcated  
8 branches. In transient nonlinear finite element (FE) codes, this material softening leads to a tangent  
9 stiffness tensor that is not positive-definite, resulting in numerical instability. This instability manifests  
10 itself as non-physical localised deformation with post-bifurcation mesh dependency (the behaviour is  
11 mesh-sensitive).  
12  
13  
14  
15  
16

17 It is well-known that the addition of a characteristic length scale to constitutive models maintains the  
18 character of the governing equations in the material softening (post-bifurcation) deformation regime. The  
19 characteristic length scale can be taken into account either in the form of spatial gradients (e.g. Dillon and  
20 Kratochvil (1970), Aifantis (1984, 1995), Zbib et al. (1992), Fleck et al. (1994), Abu Al-Rub et al. (2004),  
21 Bammann and Solanki (2010), and Solanki and Bammann (2010b)) or integral nonlocal terms (e.g. Pijaudier-  
22 Cabot and Bažant (1987), Leblond et al. (1994), Tvergaard and Needleman (1995, 1997), and Enakoutsa et  
23 al. (2007, 2012)). Furthermore, a non-local approach based on the introduction of length scale(s) provides  
24 a method for models to capture relevant aspects of the underlying physics (sub continuum scale effects) of  
25 materials.  
26  
27  
28  
29

30 Smoothed Particle Hydrodynamics (SPH) is a meshless particle method initially proposed by Lucy (1977) and  
31 Gingold and Monaghan (1977) for modelling, as the name states, hydrodynamics. The method was  
32 extended to modelling of solids with defined strength by Libersky et al. (1991, 1993). As a meshless  
33 method SPH does not require a structured grid, with the motion of the continuum approximated by  
34 motion of discrete material points (particles) with no fixed connectivity. The balance equation for mass,  
35 linear momentum and energy are discretised in space with kernel interpolation, where field variables at a  
36 particle location are approximated as a weighted (smoothed) sum of field values at the neighbouring  
37 particles. The finite domain of the kernel (smoothing) function, often called the smoothing length, defines  
38 the range of influence of an individual particle. The significant difference to the FE method is that the  
39 kernel interpolation does not satisfy the Kronecker delta condition, i.e.  $W_i(x_j) \neq \delta_{ij}$ , and that the  
40 interpolation domains are overlapping resulting in a non-unique approximation of the field variables (for  
41 details see, for instance, Libersky et al. (1991, 1993) and Swegle et al. (1994)).  
42  
43  
44  
45  
46  
47

48 The purpose of this study was to investigate if SPH is by nature a nonlocal method, capable of overcoming  
49 difficulties related to material softening without any additional regularisation measures. In this  
50 investigation a local damage model resulting in material strain-softening was used in a stable Total-  
51 Lagrange SPH code, Vignjevic et al. (2006). The investigation was done by considering a simple uniaxial  
52 wave propagation problem in a symmetrically loaded homogeneous bar, in presence of damage induced  
53 strain-softening, which is defined by Bažant and Belytschko (1985). They derived an exact solution for  
54 given initial and boundary conditions for stress wave propagation and demonstrated that for the FE spatial  
55 discretisation combined with a strain-softening material, deformation localised in a single element. With  
56  
57  
58  
59  
60  
61  
62  
63  
64  
65

strain localised in the element undergoing strain-softening, stress wave propagation through the element stopped and the rest of the bar unloaded elastically. Consequently the numerical results were dependent on the element size, i.e. showed pronounced mesh sensitivity.

The investigation presented in this paper demonstrates that this does not occur when SPH is used to analyse the same problem. It was found that stress wave propagation continues in the presence of strain-softening and the waves continue to propagate within the localisation zone. Furthermore, it is shown that in this problem the smoothing length represents a damage related length scale independent of the particle spacing (spatial discretisation density). This leads to the observation that the SPH method has inherent non-local properties.

## 2 Theoretical Background of Strain-Softening

### 2.1 Continuum Damage Mechanics

According to CDM theory, the properties of an isotropic material, including damage, have a homogeneous distribution within a representative volume element (RVE). Damage is defined by a scalar damage variable  $\omega$ , which has a value between zero and one.  $\omega = 0$  corresponds to no damage and  $\omega = 1$  corresponds to complete material failure.

One possible physical interpretation of damage is as a reduction in effective load carrying area within the RVE, as originally proposed by Kachanov (1958). In this case,  $\omega$  is expressed as the ratio of damaged surface area,  $\delta S_D$ , to the original undamaged surface area,  $\delta S$ :

$$\omega = \frac{\delta S_D}{\delta S} \quad (2-1)$$

This interpretation of damage leads to a constitutive equation expressed in terms of effective stress  $\tilde{\sigma}$ , see Rabotnov (1968). The relationship between the true stress and effective stress can then be derived from a definition of effective load carrying area  $\delta \tilde{S} = \delta S - \delta S_D$  and the force equilibrium,  $\tilde{\sigma} \delta \tilde{S} = \sigma \delta S$  as:

$$\tilde{\sigma} = \sigma \frac{1}{(1-\omega)}. \quad (2-2)$$

Making use of the effective stress, combined with equivalent strain principle, Hooke's law can be expressed in two equivalent forms, i.e.  $\sigma = \tilde{E} \varepsilon_e$  or  $\tilde{\sigma} = E \varepsilon_e$ , where  $\tilde{E}$  is the effective Young's modulus and  $\varepsilon_e$  is the elastic strain. Note that the true stress  $\sigma$  results in the same elastic strain for a damaged material as  $\tilde{\sigma}$  for the virgin material. This provides a relationship between  $\omega$  and  $\tilde{E}$ :

$$\omega = 1 - \frac{\tilde{E}}{E}, \quad \tilde{E} = E(1-\omega) \quad (2-3)$$

## 2.2 Loss of Uniqueness

The development of localised deformation is caused by a physical process occurring on a sub-continuum scale. The process is defined by the initiation, growth and interaction of cracks and voids within the material which finally lead to complete material fracture. In this investigation we use the definition of localization proposed by Rudnicki and Rice (1975): "localization is defined as instability in the macroscopic constitutive description of inelastic deformation of the material". This instability allows the constitutive equations of an originally homogeneous material to reach a bifurcation point and become unstable. Consequently the deformation localises and becomes non-uniform, while outside this instability zone the material continues to be stable, Rudicki (1975).

When the FE method, combined with a conventional local constitutive equation, is applied to model the response of a softening material the results are nonphysical and mesh dependent. This is a consequence of the ill-posed description of the governing differential equations in the material softening zone. In static problems, the partial differential equations (PDEs) change from elliptic to a hyperbolic in the softening zone, while in dynamic problems they change from hyperbolic to elliptic.

A material is considered to be stable and stay in equilibrium, when the double contraction of stress-rate  $\dot{\sigma}_{ij}$  and strain-rate  $\dot{\epsilon}_{ij}$  is positive. This criterion is also called general bifurcation criterion, Neilsen (1993), and is true as long as the stress-strain relationship of the material has a positive slope.

$$\dot{\epsilon}_{ij}\dot{\sigma}_{ij} > 0 \quad (2-4)$$

In this study we are considering the transient dynamic response of a material so the constitutive equations are written in the rate form, with a piecewise linear relationship between stress and strain rates established through the material tangent stiffness tensor  $D_{ijkl}$  as:

$$\dot{\sigma}_{ij} = D_{ijkl}\dot{\epsilon}_{kl} \quad (2-5)$$

Therefore, the inequality (2-4) reads:

$$\dot{\epsilon}_{ij}D_{ijkl}\dot{\epsilon}_{kl} > 0 \quad (2-6)$$

The material becomes unstable when the material reaches its limiting point, which occurs when the condition (2-6) is violated. This criterion defines the bifurcation point and is mathematically expressed as:

$$\dot{\epsilon}_{ij}D_{ijkl}\dot{\epsilon}_{kl} = 0. \quad (2-7)$$

The bifurcation criterion is reached when the tangent stiffness tensor becomes singular (not positive-definite) anymore:

$$\det(D_{ijkl}) = 0 \quad (2-8)$$

## 2.3 Strain-Softening

The test problem chosen to illustrate nonlocal properties of SPH is based on the 1D stress state dynamic softening problem for which Bažant and Belytschko (1985) derived an analytical solution. To make the

problem more suited to analysis codes a 1D strain was assumed, then a new analytical solution developed following procedure presented in aforementioned work.

Figure 1 shows the stress-strain curve of a general strain-softening material, as considered by Bažant and Belytschko (1985). For the linear elastic behaviour between the points O and P, the material stiffness is defined by Young's modulus  $E$ . The maximum strength  $f'_t$  is reached for the strain  $\varepsilon_p$ . The curve in the strain softening zone (between points P and F) is defined by the function  $F(\varepsilon)$ , and the slope of this part of the curve,  $F'(\varepsilon)$ , is negative. Function  $F(\varepsilon)$  reaches a zero stress for a finite strain  $\varepsilon$  or an asymptotic strain  $\varepsilon \rightarrow \infty$ . In the original paper of Bažant and Belytschko (1985), unloading ( $\dot{\varepsilon} < 0$ ) and reloading ( $\dot{\varepsilon} \geq 0$ ) is considered to be elastic and occur with the undamaged Young's modulus  $E$ .

#### NEAR Figure 1

Figure 1 Stress-strain diagram of softening material Bažant and Belytschko (1985)

The geometry and the loading conditions of the problem are shown in Figure 2. The bar length is  $2L$ , material density per unit length is  $\rho$  and the coordinate system is chosen so that the longitudinal coordinate  $x$  is measured from the bar centre. The bar is loaded at both ends with a constant velocity  $v$ , applied in opposite directions.

#### NEAR Figure 2

Figure 2: Geometry and loading of softening bar, Bažant and Belytschko (1985)

Two tensile step waves are generated in the bar, one travelling from the right boundary in the negative  $x$ -direction and the other travelling from the left boundary in the positive  $x$ -direction. These two step waves of constant strain meet in the centre of the bar ( $x = 0$ ) at time  $t = L/c_e$ . At this point the strain doubles instantaneously, and the midsection zone of the bar enters the strain-softening regime.

For elastic material response the wave equation is hyperbolic:

$$c_e^2 \frac{\partial^2 u}{\partial x^2} = \frac{\partial^2 u}{\partial t^2} \quad (2-9)$$

where  $c_e$  is the elastic wave speed, which for the 1D state of strain, is:

$$c_e = \sqrt{\frac{E(1-\nu)}{\rho(1-2\nu)(1+\nu)}} \quad (2-10)$$

The longitudinal displacement function for the linear elastic response is derived from appropriate initial and boundary conditions:

$$u(x, t) = -v \left\langle t - \frac{x+L}{c_e} \right\rangle + v \left\langle t + \frac{x-L}{c_e} \right\rangle \quad (2-11)$$

where the expressions in the brackets  $\langle \cdot \rangle$  need to be positive-definite. The corresponding strain is obtained as:

$$\varepsilon_x = \frac{\partial u}{\partial x} = \frac{v}{c_e} \left[ H \left( t - \frac{x+L}{c_e} \right) + H \left( t + \frac{x-L}{c_e} \right) \right] \quad (2-12)$$

where  $H(\cdot)$  is the Heaviside step function. The stress state induced by this deformation is:

$$\sigma_x = \frac{E(1-\nu)}{(1-2\nu)(1+\nu)} \varepsilon_x \quad (2-13)$$

This assumption of linear elasticity (2-11) only holds for  $t < L/c_e$ , before the centre of the bar enters the strain-softening regime at response time  $t = L/c_e$ , when the two stress step waves meet. At the centre of the bar, the slope of the stress-strain curve (the strain in the bar satisfies the condition:  $\varepsilon_p/2 < \varepsilon \leq \varepsilon_p$ ) becomes negative, i.e.  $F'(\varepsilon) < 0$ , and the wave speed  $c$  becomes imaginary. Consequently, the equation of motion in the softening domain becomes an elliptic PDE:

$$c^2 \frac{\partial^2 u}{\partial x^2} + \frac{\partial^2 u}{\partial t^2} = 0 \quad \text{with} \quad c^2 = \frac{F'(\varepsilon)}{\rho} \quad (2-14)$$

Theoretically, the softening is limited to an area of zero width at  $x = 0$ . So a discontinuity with a displacement jump develops at this point, giving a difference in magnitude of strain  $\varepsilon = 4v(t - L/c_e)$ . Strain increases towards infinity and stress drops to zero within the softening zone. Release waves are generated from this point and propagate into the bar.

The infinite strain in the softening domain can be expressed by the Dirac Delta function  $\delta(x)$  as:

$$\varepsilon_x = 4vt - \frac{L}{c_e} \delta(x) \quad (2-15)$$

The solution for the strain field outside the softening zone,  $t > L/c_e$  and  $x < 0$ , (consequently in  $x > 0$  part of the bar, due to symmetry of the problem), is then:

$$\varepsilon_x = \frac{v}{c_e} \left[ H \left( t - \frac{x+L}{c_e} \right) - H \left( t - \frac{L-x}{c_e} \right) + 4c_e t - Lv \delta(x) \right] \quad (2-16)$$

Following Bažant and Belytschko (1985), this analytical solution was used to derive a comparison between an elastic ( $\varepsilon \leq \varepsilon_p/2$ ) and a strain-softening ( $\varepsilon_p/2 < \varepsilon \leq \varepsilon_p$ ) wave propagation problem.

Figure 3 to Figure 6 show the solutions for longitudinal displacement, strain and stress along the bar at time  $= 3/2 \cdot L/c$ , for both the elastic and strain-softening responses of a local continuum. The elastic solution represents continuous wave propagation after superposition of the waves. The results for the strain-softening solution show clearly the consequences of strain-softening; a displacement discontinuity develops after the superposition in the localisation zone at  $x = 0$  and this zone localises in an area of zero width (see Figure 3). This discontinuity cannot propagate outside this zone, as the type of PDE in this zone has changed to elliptic and interaction with areas  $x \neq 0$ , which are governed by hyperbolic PDEs, is not possible. Consequently strain grows to infinity, as illustrated in Figure 4, and simultaneously stress in the localisation zone drops to zero, see Figure 5. Outside the localisation zone, the bar unloads as release waves travel to the bar ends. One can observe that the softening zone effectively acts as a free boundary.

**NEAR Figure 3**

Figure 3: Elastic local and nonlocal solutions for normalised longitudinal displacement at  $t = 3/2 \cdot L/c$

**NEAR Figure 4**

Figure 4: Elastic local and nonlocal solutions for normalised longitudinal strain at  $t = 3/2 \cdot L/c$

**NEAR Figure 5**

Figure 5: Elastic local and nonlocal solutions for normalised longitudinal stress at  $t = 3/2 \cdot L/c$

**NEAR Figure 6**

Figure 6: Internal energy history for the local and nonlocal solutions

### 3 Main Aspects of the Smoothed Particle Hydrodynamics (SPH) Method as Nonlocal Regularisation Method

#### 3.1 Nonlocal Regularisation

In a local theory stress only depends on the deformation history of a single point  $\mathbf{x}$ . A nonlocal theory considers additionally the influence of the deformation of surrounding points,  $\xi$ , in a representative volume element (RVE). This is done by substituting the local variable  $\eta(\mathbf{x})$  by a weighted average  $\bar{\eta}(\mathbf{x})$  of the variable in the point's spatial neighbourhood.

Nonlocal integral theory aims to describe spatial interactions with weighted spatial averages. A transformation rule is defined by an integral over a RVE domain, denoted as  $V$  in the integral below:

$$\bar{\eta}(\mathbf{x}) = \int_V \alpha(\mathbf{x}, \xi) \eta(\xi) d\xi \quad (3-1)$$

where  $\alpha(\mathbf{x}, \xi)$  is a weighting function for a local state variable in the spatial domain  $V$ .

The size of the RVE is quantified by a characteristic length  $l$ , also called the internal length. It is understood as a material property which depends on the size of material heterogeneities on the micro-scale. An example of a common weighting function  $\alpha(\mathbf{x}, \xi)$  is the Gaussian function:

$$\alpha(r) = \alpha(\|\mathbf{x} - \xi\|) = \frac{1}{(2\pi)^{3/2} l^3} \exp\left(-\frac{r^2}{2l^2}\right) \quad (3-2)$$

With increase in distance from the point  $\mathbf{x}$ , the influence of the surrounding material reduces and reaches zero at the boundaries of the RVE. This averaging process is often called smoothing.

### 3.2 Nonlocal Aspect of the SPH Method

Smoothed Particle Hydrodynamics (SPH) is a meshless Lagrangian particle method, where the motion of a continuum is described by the movement of a finite number of discrete particles, which are used in the spatial discretisation of the state variables, Lucy (1977), Gingold and Monaghan (1977). Instead of a mesh, SPH uses kernel interpolation to approximate the field variables at any point in a domain. For instance, an estimate of the value of a function  $f(\mathbf{x})$  at the location  $\mathbf{x}$ , is given in a continuous form by an integral of the product of the function and a kernel (weighting) function  $W(|\mathbf{x} - \mathbf{x}'|, h)$ :

$$\langle f(\mathbf{x}) \rangle = \int_{\Omega} f(\mathbf{x}') W(|\mathbf{x} - \mathbf{x}'|, h) d\mathbf{x}' \quad (3-3)$$

where the angle brackets  $\langle \cdot \rangle$  denote a kernel approximation,  $h$  is a parameter that defines the size of the kernel support (also known as the smoothing length), and  $\mathbf{x}'$  is a new independent variable.

The kernel function (3-3) usually has the following properties:

- Compact support, which means that it is equal to zero everywhere except within a finite domain. In conventional SPH, this domain is taken to be a sphere with a radius of twice the smoothing length,  $h$ , i.e. the domain includes all the points within a distance of two smoothing lengths,  $h$ , from the point  $\mathbf{x}'$  (see Figure 7):

$$W(|\mathbf{x} - \mathbf{x}'|, h) = 0 \quad \text{for} \quad |\mathbf{x} - \mathbf{x}'| \geq 2h \quad (3-4)$$

- Normalised:

$$\int_{\Omega} W(|\mathbf{x} - \mathbf{x}'|, h) d\mathbf{x}' = 1 \quad (3-5)$$

These requirements, formulated by Lucy (1977), ensure that the kernel function reduces to the Dirac delta function when  $h$  tends to zero:

$$\lim_{h \rightarrow 0} W(|\mathbf{x} - \mathbf{x}'|, h) = \delta(|\mathbf{x} - \mathbf{x}'|, h) \quad (3-6)$$

So therefore, it follows that:

$$\lim_{h \rightarrow 0} \langle f(\mathbf{x}) \rangle = f(\mathbf{x}) \quad (3-7)$$

If the function  $f(\mathbf{x})$  is only known at  $N$  discrete points, the integral in equation (3-3) can be approximated by a summation:

$$\begin{aligned} f_I &= f(\mathbf{x}_I) \\ &\approx \langle f(\mathbf{x}_I) \rangle = \int_{\Omega} f(\mathbf{x}') W(|\mathbf{x} - \mathbf{x}'|, h) d\Omega \approx \sum_{j=1}^N \frac{m_j}{\rho_j} f(\mathbf{x}_j) W(|\mathbf{x}_I - \mathbf{x}_j|, h) \end{aligned} \quad (3-8)$$

In the equation above, the subscripts  $I$  and  $J$  denote particle numbers,  $m_J$  and  $\rho_J$  are, respectively, the mass and the density of particle  $J$ ,  $N$  is the number of neighbours of particle  $I$  (number of particles that interact with particle  $I$ , i.e. within the support of the kernel), and  $m_J/\rho_J$  is the volume associated to the point or particle  $J$ . Equation (3-8) constitutes the basis of the SPH method, where the value of a field variable at particle  $I$  is approximated by summing the weighted field values from a set of neighbouring particles, denoted by subscript  $J$ .

In the SPH literature, the term particles is misleading as these particles in fact have to be thought of as interpolation points rather than mass elements. Furthermore it is important to observe that the kernel interpolation does not satisfy the Kronecker delta condition, i.e.  $W_i(x_j) \neq \delta_{ij}$  and that the interpolation domains are overlapping resulting in a non-unique approximation of the field variables (for details see, for instance, Libersky at al. (1991, 1993) and Swegle at al. (1994)).

### NEAR Figure 7

Figure 7: Set of neighbouring particles

Using basic properties of the kernel approximation, a discrete form of a spatial derivative approximation can be derived as:

$$\langle \nabla f(x_I) \rangle = \sum_J \frac{m_J}{\rho_J} f(x_J) [\nabla W(|x_I - x_J|, h)] \quad (3-9)$$

The SPH approximations of field variables are values smoothed over the kernel function domains or, in its discrete form, over a number of neighbours for a given particle  $I$ . This kernel smoothing/interpolation gives the SPH method nonlocal properties. More specifically, the density, stress and velocity fields in SPH are smoothed (discretised) using the kernel interpolation. Furthermore, in SPH the constitutive equations are integrated for all particles, i.e. all particles carry information about density, velocity, stress and internal state variables, which makes the method collocational. In FE, based on the isoparametric element formulation, constitutive equations are integrated at the Gauss points and the discrete values for the velocity field are determined for nodal points, which makes this method non-collocational.

Although frequently used, the conventional SPH method based on an Eulerian kernel, e.g. Libersky at al. (1993), suffers from an instability commonly known as the 'tensile instability', which was first investigated by Swegle (1994). This instability manifests itself as the development of unphysical fractures or as clumping together of particles, when the material is subjected to tension. Belytschko at al. (2000) and Vignjevic at al. (2006) showed that the tensile instability associated with the use of an Eulerian kernel can be avoided by using a Total Lagrangian kernel. An outline of a stable Total Lagrangian form of SPH, used in this work, is given below, whilst the full information about this form of SPH can be found in Vignjevic at al. (2006).

In the Total Lagrangian formulation the balance equations are written in the initial configuration and expressed in terms of material coordinates. The Total Lagrangian SPH form of the discretised balance equations are given in Table 3.1, Vignjevic at al. (2006). These equations are discretised using the Total

Lagrangian kernel function and its derivatives are evaluated in the initial configuration, in terms of the initial coordinates  $x_i^0$  and  $x_j^0$  of the  $i$  and  $j$  particles.

Table 3.1 Balance equations in continuum and SPH discrete forms Vignjevic at al. (2006)

**NEAR Table 3.1**

Where:  $\mathbf{F}$  is deformation gradient,  $J = \det \mathbf{F}$  is the Jacobian of deformation gradient,  $\rho$  is material density,  $\mathbf{u}$  is displacement,  $\mathbf{P}$  is first Piola-Kirchhoff stress,  $\mathbf{b}$  is a body force per unit mass,  $e$  is internal energy. The superscript  $^0$  in the equation above indicates initial configuration and dot above a variable denotes time derivative.

This SPH discretisation results in the following equation for the deformation gradient, Vignjevic at al. (2006):

$$\langle \mathbf{F}_i \rangle = - \sum_{j=1}^{np} \frac{m_j}{\rho_j^0} (\mathbf{v}_i - \mathbf{v}_j) \otimes \nabla_{\mathbf{x}_i^0} W(|\mathbf{x}_i^0 - \mathbf{x}_j^0|, h^0) \quad (3-10)$$

A normalised corrected version of SPH based on cubic B-spline kernel function was used (for more details, see Vignjevic at al. (2000)). These semi-discretised equations are integrated in time using a central difference integration scheme (explicit time integration). The update of particle positions was performed using a smoothed velocity (XSPH), Randles and Libersky (1996).

## 4 Numerical Experiments for the Evaluation of the SPH Method

The objective of the numerical experiments was to investigate the behaviour of the SPH method, when used with a local CDM material model with strain-softening. Then to compare the results with equivalent analyses performed with the FE method. The tests were conducted with an in-house Total-Lagrangian SPH code (MCM) and with the FE code DYNA3D, Lin (2004), available at Cranfield University. The 1D strain, wave propagation problem, described in section 2.3 was used as the benchmark example.

### 4.1 Material Model

An isotropic elastic material model with damage was used in this study, with a stress-strain relationship is illustrated in Figure 8. The onset of strain-softening occurs when strain reaches the damage initiation strain  $\varepsilon_i$ , which corresponds to the maximum strength. After the onset of strain-softening, material strength reduces gradually until it reaches zero at a strain equal to the critical failure strain  $\varepsilon_f$ .

**NEAR Figure 8**

Figure 8: Material model with strain-softening implemented into the MCM SPH code and FE code DYNA3D

The evolution of the damage variable was defined to give linear stress-strain behaviour following the onset of damage growth. In the model,  $E$  is the Young's modulus of a virgin material, which defines material linear elastic behaviour. Material stiffness in the softening regime is defined by the tangent stiffness (softening part of the stress strain curve),  $E_t$ . Material loading/unloading response in the softening regime was defined using the secant stiffness, denoted as  $\tilde{E} = E$ . The secant stiffness is equivalent to virgin material Young's modulus. The parameters  $\varepsilon_i$  and  $\varepsilon_f$  define the initiation and critical failure strains, respectively, and  $\varepsilon^*$  denotes the current strain.

The stiffness of the softening material was defined by the slope of the strain-softening part of the stress-strain curve:

$$E_t = \frac{-E\varepsilon_i}{\varepsilon_f - \varepsilon_i} \quad (4-1)$$

Using equation (2-2) damage variable  $\omega$  can then be expressed as:

$$\omega = \frac{\varepsilon_f (\varepsilon^* - \varepsilon_i)}{\varepsilon^* (\varepsilon_f - \varepsilon_i)} \quad (4-2)$$

For  $\varepsilon^* = \varepsilon_i$ ,  $\omega = 0$  and for  $\varepsilon^* = \varepsilon_f$ , i.e. at the point of material failure  $\omega_f = 1$ .

## 4.2 Numerical Test Setup

A number of numerical tests were performed to illustrate the inherent nonlocal properties of the SPH method, where the smoothing length, in addition to its interpolation meaning, represents material characteristic length.

The bar, used in the numerical experiments, has an overall length of  $2l = 200$  mm and a square cross section. In the SPH models symmetry planes are used to properly enforce the boundary conditions on the long edges. The origin of the coordinate system was located in the centre of the bar with the  $x$  axis aligned with the bar. All degrees of freedom except for the longitudinal direction are restricted in order to ensure uniaxial strain conditions. The material input data used in the simulations is given in Table 4.1.

Table 4.1: Input data for isotropic CDM model with linear strain-softening for FE (DYNA3D) and SPH (MCM) codes

NEAR Table 4.1

The bar was loaded in tension by applying constant velocity in opposite directions to its ends. In order to induce the softening regime in material, the applied velocity has to be between  $v_{min} = \frac{\varepsilon_f}{2} \cdot c_e$  and  $v_{max} = \varepsilon_f \cdot c_e$ . Consequently, for the elastic wave speed  $c_e = 7357730.67 \text{ mm/s}$ , calculated from (2-12), the constant velocity applied in all simulations is  $v_{const.} = 7 \times 10^4 \text{ mm/s}$ .

To provide a reference data set for comparison with SPH, and to illustrate the mesh dependency of the FE model, the bar problem was simulated with the nonlinear transient FE code DYNA3D, using the local constitutive model described in Section 4.1. Four different spatial discretisations (mesh densities) were considered: the bar was discretised with 31, 101 151 and 201 elements along x axis, as shown in Figure 9.

**NEAR Figure 9**

Figure 9: Spatial discretisations used in the FE (DYNA3D) simulation of the strain-softening bar

Similarly, in the SPH simulations, the bar was discretised with three different particle densities, determined by inter-particle spacings:  $\Delta p = 1.98, 1.32$  and  $0.995$  mm, as shown in Figure 10.

**NEAR Figure 10**

Figure 10: Particle discretisation in SPH (MCM) of strain-softening bar

The smoothing length, which determines the range over which particle velocities and stresses are smoothed, is defined as:

$$h = \lambda \cdot \Delta p \quad (4-3)$$

where  $\lambda$  is a factor, which relates the interparticle spacing to the smoothing length. For the B-Spline kernel, the smoothing domain has radius  $2h$ , which is user defined parameter in SPH simulations.

The influence of the smoothing length on the results is illustrated with three numerical experiments summarised in Table 4.2.

- The first experiment investigates the influence of variable  $h$ , where  $h$  was varied by changing the interparticle distance  $\Delta p$  while keeping parameter  $\lambda$  constant at  $\lambda = 1.3$ . This is a typical value used in SPH analyses. In this experiment, the number of neighbours for a given particle, i.e. particles that lie within a spherical domain of radius  $2h$ , was the same for all models.
- The second experiment investigates the influence of  $h$  on the size of softening zone in the case of constant discretisation density (interparticle distance). The interparticle distance was fixed as  $\Delta p = 200\text{mm}/201$ , and  $\lambda$  varied. Parameter  $\lambda$  was given values of  $\lambda = 1.25, 2.25$  and  $3.25$ , corresponding to 5, 9 and 13 neighbour particles in the loading direction, respectively.
- The third experiment investigated a fixed smoothing length of  $h = 2.5\text{mm}$  for different discretisation densities. In these tests, both the smoothing length parameter,  $\lambda$  and the interparticle distance  $\Delta p$ , were varied.

Table 4.2: Summary of the SPH discretisation parameters used in the three numerical experiments

**NEAR Table 4.2**

### 4.3 Numerical Results of the Strain-Softening in FE and SPH

#### 4.3.1 Strain-Softening in FE

The conventional strain-softening solutions, obtained with FE, are compared with the analytical solution for longitudinal displacement, strain and stress. The stress-strain curves, obtained at the elements located at  $x = 0$  for the FE models with different mesh densities, are shown in Figure 11. The damage was limited to this element only and propagates towards the bar ends by the deformation of this element which undergoes softening. The size of these elements, i.e. softening zones at response time  $t = 3/2 \cdot L/c_e$  is shown in Figure 12 and Figure 17. The size of the softening zone in which damage accumulates, was influenced by the initial element size (mesh sensitive).

Figure 13, Figure 14 and Figure 15 respectively show the analytical solution and the FE numerical results for longitudinal displacement, strain and stress at response time  $t = 3/2 \cdot L/c_e$ . The results show a strong dependence on the mesh density in the strain-softening area  $-L/2 \leq x \leq L/2$ , as a consequence of the local strain-softening. It can be observed that numerical results are converging to the analytical solution with the increase in mesh density. The areas outside of  $-L/2 \leq x \leq L/2$  are still governed by the elastic solution.

#### NEAR Figure 11

Figure 11: Longitudinal stress vs. longitudinal strain curves for the central element for different FE mesh densities

#### NEAR Figure 12

Figure 12: Damage distribution for different FE mesh densities at response time  $t = 3/2 \cdot L/c_e$

#### NEAR Figure 13

Figure 13: Analytical solution and FE results for longitudinal displacement at  $t = 3/2 \cdot L/c_e$

#### NEAR Figure 14

Figure 14: Analytical solution and FE results for longitudinal strain at  $t = 3/2 \cdot L/c_e$

#### NEAR Figure 15

Figure 15: Analytical solution and FE results for longitudinal stress at  $t = 3/2 \cdot L/c_e$

#### NEAR Figure 16

Figure 16: FE results for internal energy

Figure 17 illustrates the size of the strain/damage localisation zone at response time  $t = 3/2 \cdot L/c_e$ . It can be clearly seen that strain grows in a single element. Consequently, the localisation zone reduces in size with the increase in mesh density and the strain magnitude in the central element increases with the reduction in element size.

#### NEAR Figure 17

Figure 17: Strain localisation at response time  $t = 3/2 \cdot L/c_e$  in a single element due to material strain-softening (fringe level: strain [-]).

### 4.3.2 Strain-Softening in SPH

#### *Experiment 1 - Influence of interparticle distance, $\Delta p$ =variable, $\lambda = 1.3$ =constant*

The smoothing length,  $h = 1.3 \cdot \Delta p$ , was varied in these three test cases by changing the inter particle distance, while maintaining a constant number of neighbouring particles. Figure 18 shows the stress-strain curves, obtained for the central particle of the bar ( $x = 0$ ). It is clear that for all particle densities, strain-softening behaviour initiates at the centre of the bar and propagates outwards.

Figure 19 shows the distribution of damage at response time  $t = 3/2 \cdot L/c_e$ . It can be seen that the width of the damaged area depends on the chosen interparticle distance, as the smoothing length is a function of  $\Delta p$  as  $\lambda$  is constant. The damage affected zone was largest for the largest  $\Delta p$ .

Figure 20, Figure 21 and Figure 22 respectively show the profiles of longitudinal displacement, strain and stress, plotted along the bar length for the three inter-particle distances, along with the analytical solution. These results indicate that the stress waves continue to propagate through the softening zone and are close to the nonlocal solution. Damage stays limited to the softening zone.

#### NEAR Figure 18

Figure 18: Longitudinal stress vs. longitudinal strain curves at the central particle obtained with different particle densities, SPH-experiment 1.

#### NEAR Figure 19

Figure 19: Damage distribution for different particle densities at response time  $t = 3/2 \cdot L/c_e$ ; SPH-experiment 1.

#### NEAR Figure 20

Figure 20: Analytical solution and numerical results for longitudinal displacement at  $t = 3/2 \cdot L/c_e$ ; SPH-experiment 1.

#### NEAR Figure 21

Figure 21: Analytical solution and numerical results for longitudinal strain at  $t = 3/2 \cdot L/c_e$ ; SPH-experiment 1.

#### NEAR Figure 22

Figure 22: Analytical solution and numerical results for longitudinal stress at  $t = 3/2 \cdot L/c_e$ ; SPH-experiment 1.

#### NEAR Figure 23

Figure 23: Internal energy for  $0 \leq t \leq 2 \cdot L/c$ ; SPH-experiment 1.

Figure 24 shows a graphical representation of the damage zone at response time  $t = 3/2 \cdot L/c_e$ . Damage is averaged over five particles along the length of the bar. This number is constant for all particle spacings ( $\Delta p$ ) considered, however this may be difficult to observe in Figure 24 because of the significant difference in maximum damage magnitude (see Figure 19). The width of the damage zone depends on the chosen interparticle distance.

**NEAR Figure 24**

Figure 24: Localisation of damage within a limited area  $4h$  in size  $h = 1.3 \cdot \Delta p$  around the bar symmetry plane at response time  $t = 3/2 \cdot L/c_e$  (fringe level: damage [-]). SPH experiment 1

Development of damage in the centre of the bar, presented in Figure 24, shows that the increase of the smoothing length results in increase of the size of the damage zone.

**Experiment 2 - Influence of averaging over several neighbouring particles,  $\Delta p = \text{constant}$ ,  $\lambda = \text{variable}$** 

This experiment demonstrates the effects of the smoothing length size, varied by changing the parameter  $\lambda$  and keeping constant the inter-particle distance. The bar with inter-particle distance  $\Delta p = 200\text{mm}/201$  was used in these experiments with  $\lambda = 1.25, 2.25$  and  $3.25$ , which correspond to 5, 9 and 13 neighbouring particles respectively.

Again, the particles in the centre of the bar undergo strain-softening, as illustrated in the longitudinal stress - longitudinal strain curves in Figure 25. The damage distribution at response time  $t = 3/2 \cdot L/c_e$ , shown in Figure 26, indicates that the size of the damaged (softening zone) was dependent on the size of the smoothing domain. Furthermore, maximum peak value of damage was obtained with the smallest smoothing length.

Figure 27, Figure 28, Figure 29 and Figure 30 respectively show the profiles of longitudinal displacement, strain and stress plotted along the bar length for the three particle densities, along with the analytical solution. These results indicate that the stress waves continue to propagate through the softening zone and are close to the nonlocal solution. Damage stays limited to the softening zone.

**NEAR Figure 25**

Figure 25: Longitudinal stress vs. longitudinal strain curves for the central particle obtained with different values of  $\lambda$ ; SPH-experiment 2

**NEAR Figure 26**

Figure 26: Damage distribution obtained with different values of smoothing lengths at response time  $t = 3/2 \cdot L/c_e$ ; SPH-experiment 2.

**NEAR Figure 27**

Figure 27: Analytical solution and the numerical results for longitudinal displacement at response time  $t = 3/2 \cdot L/c_e$ ; SPH-experiment 2.

**NEAR Figure 28**

Figure 28: Analytical solution and the numerical results for longitudinal strain at response time  $t = 3/2 \cdot L/c_e$ ; SPH-experiment 2.

**NEAR Figure 29**

Figure 29: Analytical solution and the numerical

**NEAR Figure 30**

Figure 30: Internal energy for  $0 \leq t \leq 2 \cdot L/c$ ; SPH

results for longitudinal stress at response time experiment 2.

$t = 3/2 \cdot L/c_e$ ; SPH experiment 2.

Figure 31 shows the size of the damage zone, at response time  $t = 3/2 \cdot L/c_e$ , obtained in the SPH experiment 2. The three models have the same interparticle distance  $\Delta p = 200mm/201$ ; however, the smoothing distance  $h$  was varied and consequently the number of neighbouring particles increased with increase of  $\lambda$ .

#### NEAR Figure 31

Figure 31: Localisation of damage within a limited area  $4h$  in size ( $h = \lambda \cdot 200mm/201$ ) around the bar symmetry plane at response time  $t = 3/2 \cdot L/c_e$  (fringe level plotted on the scaled particles for the sake of clarity: damage [-]); SPH experiment 2.

#### **Experiment 3 - Influence of constant smoothing length, $\Delta p = \text{variable}$ , $\lambda = \text{variable}$ , $h = 2.5 \text{ mm}$**

Experiment 3 demonstrates the behaviour of SPH for different interparticle distances, subjected to a fixed smoothing length size,  $h = 2.5mm$ . The particle density, i.e. the number of neighbouring particles, was changed, by varying the interparticle distance used in the model. Figure 32 shows the stress-strain curves for the three particle densities considered. It is clear that all bars underwent linear strain-softening behaviour.

Damage distribution at response time  $t = 3/2 \cdot L/c_e$  is shown in Figure 33 for the central particle of the bar. The results indicate that the size of the damaged zone did not depend on the interparticle distance  $\Delta p$ , i.e. particle density. However the damage peak value was dependant on particle density (the lowest value obtained for the highest particle density).

The distribution of longitudinal displacement, longitudinal strain and longitudinal stress shown in Figure 34, Figure 35 and Figure 36, respectively, corroborate the above statement and are independent of the particle density. The effects of damage are smoothed out over an increasing number of particles with increasing interparticle distance. These results indicate that the stress waves continue to propagate through the softening zone and are close to the nonlocal solution.

#### NEAR Figure 32

Figure 32: Longitudinal stress vs. longitudinal strain curves for the central particle obtained with different values of  $\Delta p$ ; SPH-experiment 3.

#### NEAR Figure 33

Figure 33: Damage distribution obtained with different particle densities at response time  $t = 3/2 \cdot L/c_e$ ; SPH-experiment 3.

#### NEAR Figure 34

Figure 34: Analytical solution and the numerical

#### NEAR Figure 35

Figure 35: Analytical solution and the numerical

results for longitudinal displacement at response time  $t = 3/2 \cdot L/c_e$ ; SPH-experiment 3.

results for longitudinal strain at response time  $t = 3/2 \cdot L/c_e$ ; SPH-experiment 3.

### NEAR Figure 36

Figure 36: Analytical solution and the numerical results for longitudinal stress at response time  $t = 3/2 \cdot L/c_e$ ; SPH-experiment 3.

### NEAR Figure 37

Figure 37: Internal energy for  $0 \leq t \leq 2 \cdot L/c$ ; SPH experiment 3.

Finally, the physical size of the damage area, shown in Figure 38, is constant with a finite size of  $4h = 10mm$  and is independent of the interparticle distance.

### NEAR Figure 38

Figure 38: Localisation of damage within a limited area  $4h$  in size ( $h = 2.5mm$ ) around the bar symmetry plane at response time  $t = 3/2 \cdot L/c_e$  (fringe level: damage [-]); the damage distribution is independent of the interparticle distance  $\Delta p$ ; SPH experiment 3.

Together the results from experiments 2 and 3 show that the width of the damage zone is dependent on the smoothing length  $h$ , not the interparticle distance  $\Delta p$ . This suggests that when modelling a problem including material damage the smoothing length should not be smaller than the characteristic length of the damage and should be set to the characteristic length if the particle resolution permits.

## 5 Conclusion

In the FE simulations of the softening bar, the strain-softening process was always localised in a single element. Consequently, the results obtained using the FE method were highly mesh sensitive and non-physical. Stress waves did not propagate through the softening zone.

In the SPH simulations of the softening bar, damage was spread over the smoothing domain used in the kernel interpolation. Consequently, the smoothing domain size represents a material characteristic length. The user can control the localisation process by varying the smoothing length  $h$ . Stress waves propagated through the softening zone.

These results demonstrate that, in the problem considered, SPH performed as nonlocal method and did not suffer from the same instabilities as FE. The sensitivity of results to the spatial discretisation can be removed in SPH by adjusting the smoothing length appropriately, as the smoothing length represents a characteristic length that controls damage/softening localisation. Consequently physically representative values for a material should be used when modelling damage.

### Summary of the numerical experiments performed with SPH

The influence of the smoothing length on the strain-softening process was investigated in three different numerical experiments:

- The first experiment ( $\Delta p$ =variable,  $\lambda$ =constant=1.3) investigated the influence of the smoothing length  $h$  ( $h = \lambda \cdot \Delta p$ ) on the bar softening. The strain-softening effects were averaged over the same number of neighbouring particles for the three particle densities considered. The size of the

softening zone was defined by  $h$  and the size of the zone increased with the increase in particle size.

- The second experiment ( $\Delta p = \text{constant}$ ,  $\lambda = \text{variable}$ ) investigated the influence of variation of smoothing length  $h$ , when particle density was kept the same (constant interparticle distance). The increase in size of  $h$  resulted in reduction of the damage peak value.
- The third experiment ( $\Delta p = \text{constant}$ ,  $\lambda = \text{variable}$ ,  $h = 2.5 \text{ mm}$ ) considered a fixed size smoothing length  $h$  for three different particle densities. The damage effects propagated the same distance in all simulations, giving a constant softening zone size. The peak damage value reduced with the increase of the number of neighbouring particles.

## References

1. Abu Al-Rub, R.K. and Voyiadjis, G.Z., 2004. "Analytical and Experimental Determination of the Material intrinsic Length Scale of Strain Gradient Theory from Micro- and Nano-Indentation Experiments," *International Journal of Plasticity*, 20(6), 1139-1182
2. Aifantis, E.C., 1984. "On the Microstructural Origin of Certain Inelastic Models," *Journal of Engineering Materials and Technology*, 106, 326-334
3. Aifantis, E.C., 1995. "From Micro-Plasticity to Macro-Plasticity: The Scale- Invariance Approach," *Journal of Engineering Materials and Technology*, 117 (4), 352-355
4. Bammann, D.J. and Solanki, K., 2010. "On Kinematic, Thermodynamic and Coupling of a Damage Theory for Polycrystalline Material," *International Journal of Plasticity*, 26(6), 775-793
5. Bažant, Z. P. and Belytschko, T. B., 1985. "Wave Propagation In A Strain- Softening Bar: Exact Solution," *Journal of Engineering Mechanics*, 111 (3), 381-389
6. Bažant, Z.P. and Pijaudier-Cabot, G., 1988. "Nonlocal Continuum Damage, Localization, Instability and Convergence," *Journal of Applied Mechanics*, 55, 287-293
7. Belytschko, T., Guo, Y., Liu, W.K., Xiao, S.P., 2000. "A Unified Stability Analysis of Meshless Particle Methods", *International Journal for Numerical Methods in Engineering*, 48, 1359-1400
8. Dillon, O.W. and Kratochvill, J., 1970. "A Strain Gradient Theory of Plasticity," *International Journal of Solids and Structures*, 6, 1533-1566
9. Enakoutsa, K., Leblond, J.B. and Perrin, G., 2007. "Numerical Implementation and Assessment of a Phenomenological Nonlocal Model of Ductile Rupture," *Computer Methods in Applied Mechanics and Engineering*, 196, 1946-1957
10. Enakoutsa, K., Solanki, K., Bammann, D. and Ahad, F., 2012. "Using Damage Delocalization to Model Localization Phenomena in Bammann-Chiesa-Johnson Metals," *Journal of Engineering Materials and Technology*, 134(4)
11. Fleck, N.A., Muller, G.M., Ashby, M.F., and Hutchinson, J.W., 1994. "Strain Gradient Plasticity: Theory and Experiment," *Acta Metallurgica et Materialia*, 42(2), 475-487
12. Gingold, R.A. and Monaghan, J.J. 1977. "Smoothed particle hydrodynamics – Theory and application to non-spherical stars", *Monthly Notices of the Royal Astronomical Society*, 181, 375-389
13. Kachanov, L.M., 1958. "Time of the rupture process under creep conditions", *Izv Akad Nauk SSR Otd Tech Nauk*, 8(8), 26-31
14. Lucy, L.B., 1977. "A numerical approach to the testing of the fission hypothesis". *Astronomical Journal*, 82, 1013-1024

15. Libersky, L.D. and Petschek, A.G., 1991. "Smooth Particle Hydrodynamics with Strength of Materials". In: Trease HE, Fritts MJ and Crowley WP, editors. *Advances in the Free-Lagrange Method Including Contributions on Adaptive Gridding and the Smooth Particle Hydrodynamics Method*. USA: Springer, 248-257
16. Libersky, L.D., Petschek, A.G., Carney, T.C., Hipp, J.R. and Allahdadi, F.A., 1993. "High Strain Lagrangian Hydrodynamics a three-dimensional SPH Code for Dynamic Material Response", *Journal of Computational Physics*, 109(1), 67-75
17. Lin, J.I., 2004. "DYNA3D: A nonlinear, explicit, three-dimensional finite element code for solid and structural mechanics User manual" Lawrence Livermore National Laboratory
18. Neilsen, M. K. and Schreyer, H. L., 1993. "Bifurcations in Elastic-Plastic Materials", *International Journal of Solids and Structures*, 30 (4), 521-544
19. Pijaudier-Cabot, G. and Bažant, Z.P., 1987. "Nonlocal Damage Theory", *Journal of Engineering Mechanics*, ASCE , 113, 1512-1533
20. Ramaswamy, S. and Aravas, N., 1998. "Finite Element Implementation of Gradient Plasticity Models part I: Gradient-Dependent Yield Functions," *Computer Methods in Applied Mechanics and Engineering*, 163, 11-32
21. Rabotnov, Y. N., 1968. "Creep Rupture", 12th International Congress of Applied Mechanics, Stanford, Springer-Verlag, Berlin, 342
22. Rudnicki, J. W. and Rice, J. R., 1975. "Conditions for the Localization of Deformation in Pressure-Sensitive Dilatant Materials", *Journal of Mechanics and Physics of Solids*, 23, 371-394
23. Randles, P.; Libersky, L., 1996. "Smoothed Particle Hydrodynamics: Some Recent Improvements and Applications", *Computer Methods in Applied Mechanics and Engineering*, 139, 375-408
24. Solanki, K. and Bammann, D.J., 2010. "A Thermodynamic Framework for a Gradient Theory of Continuum Damage," *Acta Mechanica*, 213, 27-38
25. Swegle, J.W., Attaway, S.W., Heinstejn, M.W., Mello, F.J. and D.L. Hicks D.L., 1994. "An Analysis of Smoothed Particle Hydrodynamics", Sandia Report, SAND93-2513
26. Tvergaard, V. and Needleman, A., 1995. "Effects of Nonlocal Damage in Porous Plastic Solids," *International Journal of Solids Structures*, 32, 1063-1077
27. Tvergaard, V. and Needleman, A., 1997. "Nonlocal Effects on Localization in a Void-sheet", *International Journal of Solids Structures*, 34, 2221-2238
28. Vignjevic, R., Campbell, J. and Libersky, L., 2000. "A Treatment of Zero-Energy Modes in the Smoothed Particle Hydrodynamics Method", *Computer Methods in Applied Mechanics and Engineering*, 184(1), 67-85
29. Vignjevic, R, Reveles, J.R. and Campbell, J., 2006. "SPH in a Total Lagrangian Formalism". *CMES: Computer Modeling in Engineering & Sciences*, 14(3), 181-198
30. Vignjevic, R., Campbell, J., Jaric, J. and Powell, S., 2009; "Derivation of SPH Equations in a Moving Referential Coordinate System, *Computer Methods in Applied Mechanics and Engineering* , 198, 2403–2411
31. Zbib, H.M. and Aifantis, E.C., 1992. "On the Gradient-Dependent Theory of Plasticity and Shear Banding", *Acta Mechanica*, 92, 209-225

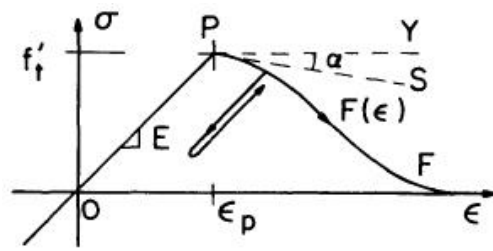


Figure 1 Stress-strain diagram of softening material Bažant and Belytschko (1985)

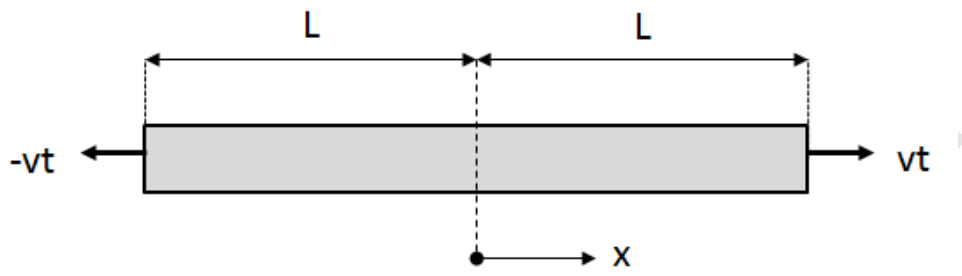


Figure 2 Geometry and loading of softening bar, Bažant and Belytschko (1985)

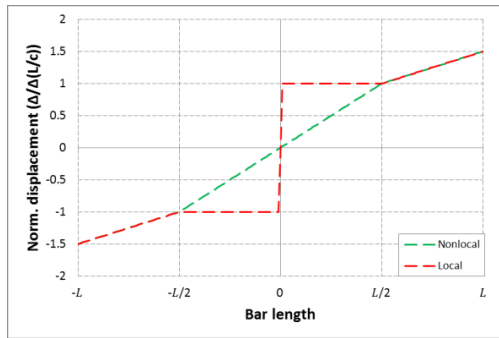


Figure 3 Elastic local and nonlocal solutions for normalised longitudinal displacement at  $t = 3/2 \cdot L/c$

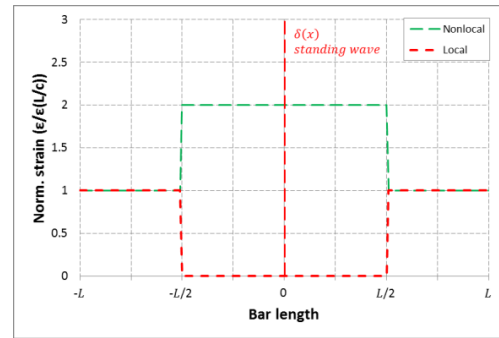


Figure 4 Elastic local and nonlocal solutions for normalised longitudinal strain at  $t = 3/2 \cdot L/c$

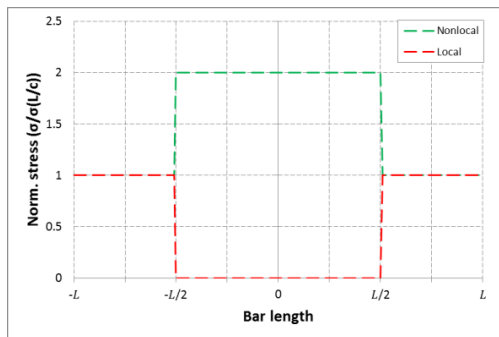


Figure 5 Elastic local and nonlocal solutions for normalised longitudinal stress at  $t = 3/2 \cdot L/c$

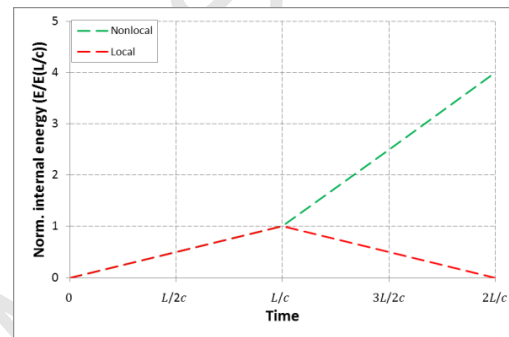


Figure 6 Internal energy history for the local and nonlocal solutions

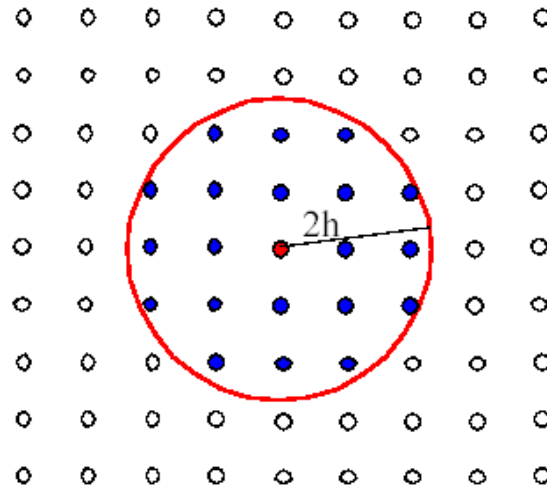


Figure 7 Set of neighbouring particles

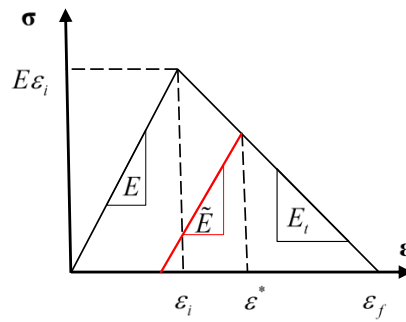


Figure 8 Material model with strain-softening implemented into the MCM SPH code and FE code DYN3D

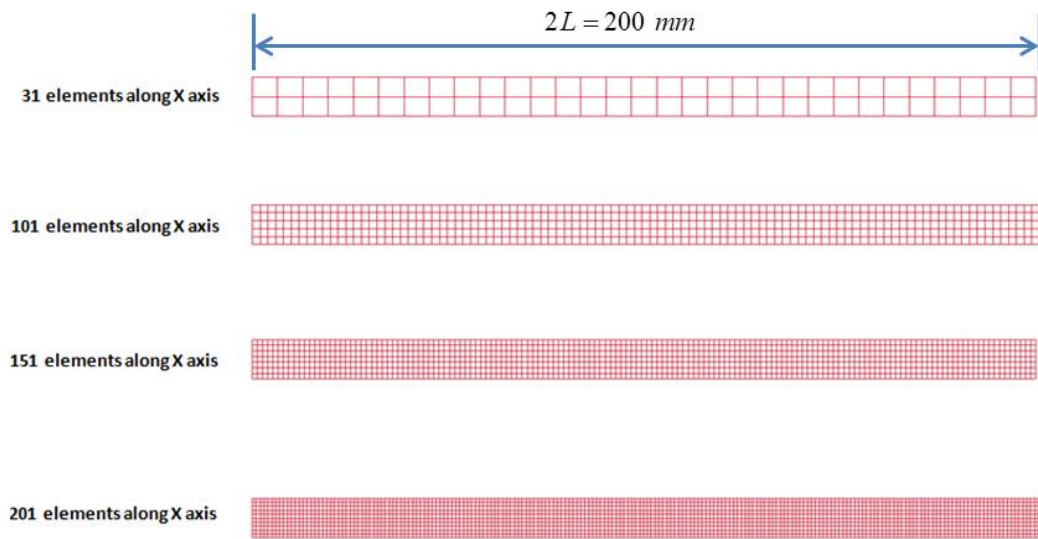


Figure 9 Spatial discretisations used in the FE (DYNA3D) simulation of the strain-softening bar

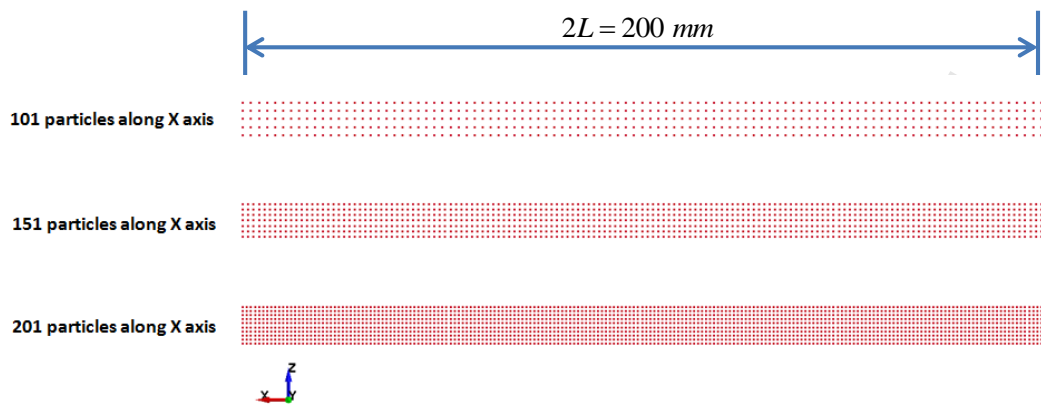


Figure 10 Particle discretisation in SPH (MCM) of strain-softening bar

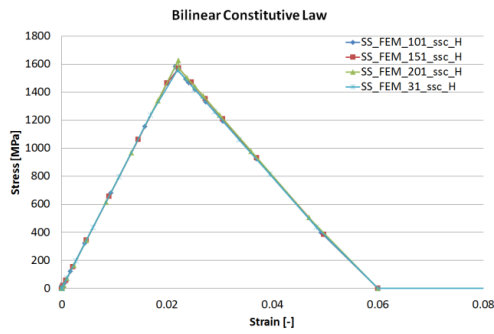


Figure 11 Longitudinal stress vs. longitudinal strain curves for the central element for different FE mesh densities

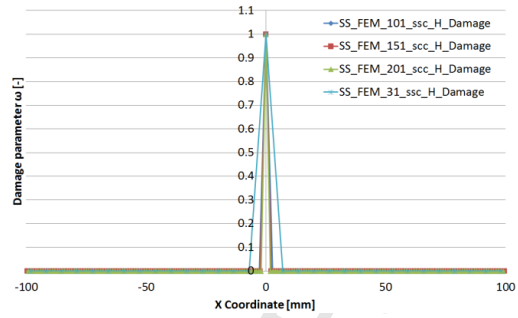


Figure 12 Damage distribution for different FE mesh densities at response time  $t = 3/2 \cdot L/c_e$

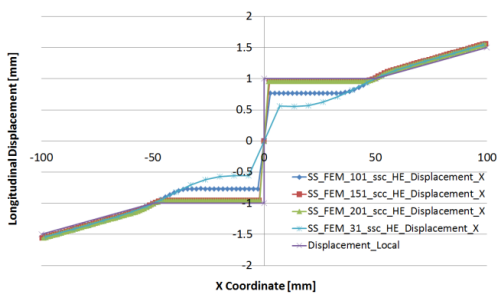


Figure 13 Analytical solution and FE results for longitudinal displacement at  $t = 3/2 \cdot L/c_e$

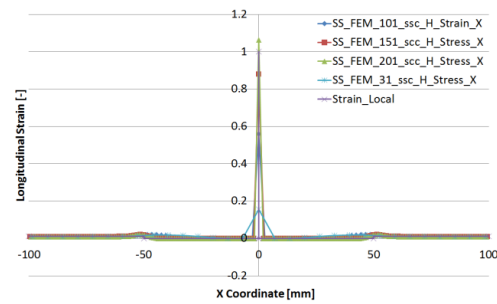


Figure 14 Analytical solution and FE results for longitudinal strain at  $t = 3/2 \cdot L/c_e$

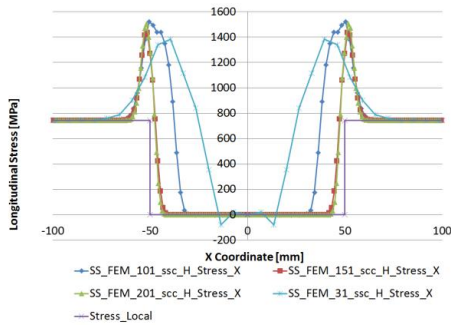


Figure 15 Analytical solution and FE results for longitudinal stress at  $t = 3/2 \cdot L/c_e$

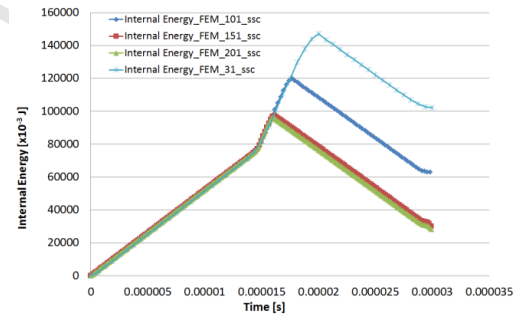


Figure 16 FE results for internal energy

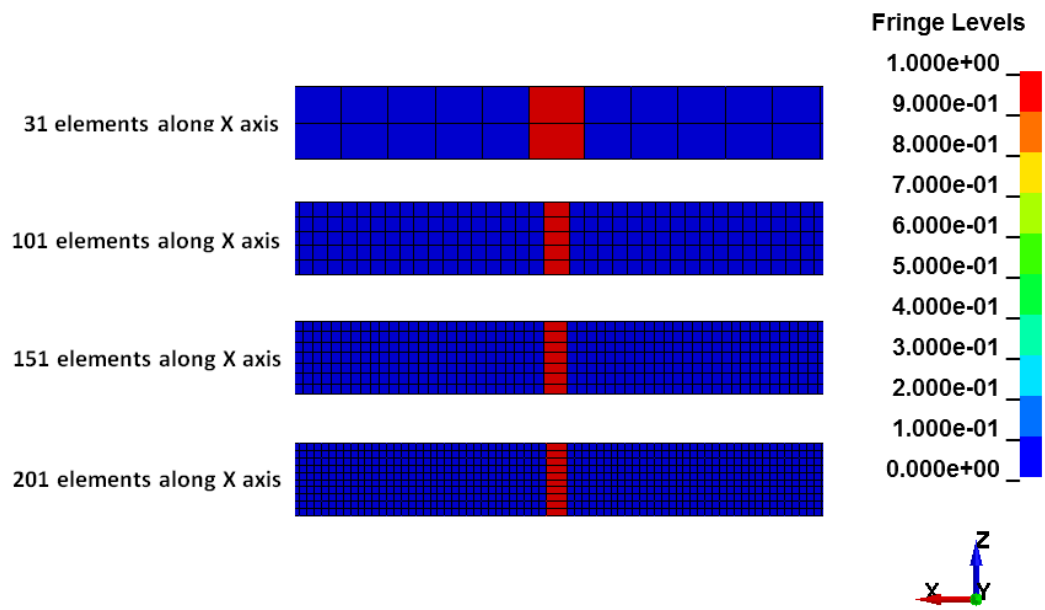


Figure 17 Strain localisation at response time  $t = 3/2 \cdot L/c_e$  in a single element due to material strain-softening (fringe level: strain [-])

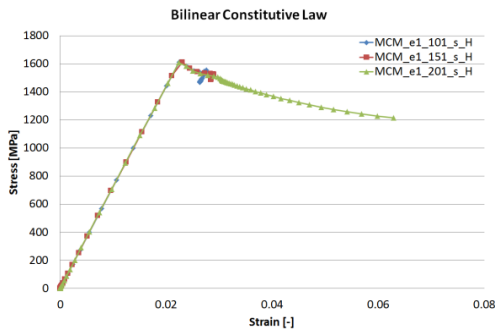


Figure 18 Longitudinal stress vs. longitudinal strain curves at the central particle obtained with different particle densities, SPH-experiment 1.

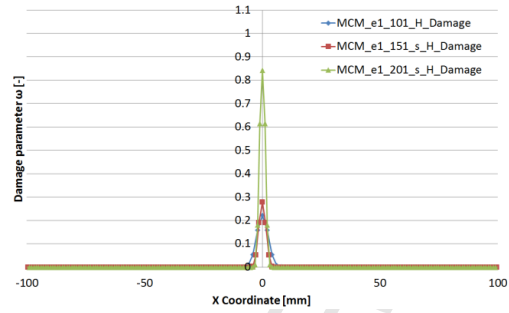


Figure 19 Damage distribution for different particle densities at response time  $t = 3/2 \cdot L/c_e$ ; SPH-experiment 1.

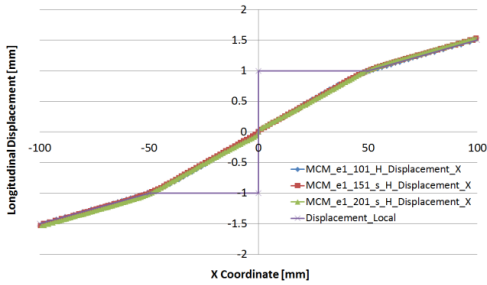


Figure 20 Analytical solution and numerical results for longitudinal displacement at  $t = 3/2 \cdot L/c_e$ ; SPH-experiment 1.

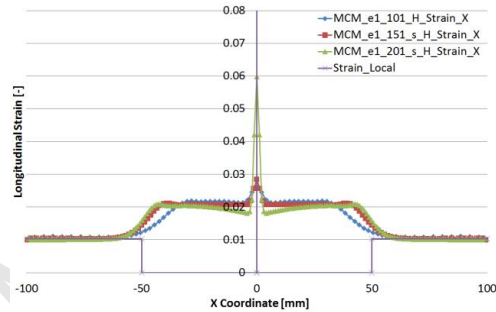


Figure 21 Analytical solution and numerical results for longitudinal strain at  $t = 3/2 \cdot L/c_e$ ; SPH-experiment 1.

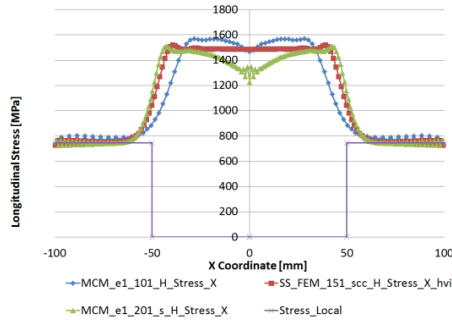


Figure 22 Analytical solution and numerical results for longitudinal stress at  $t = 3/2 \cdot L/c_e$ ; SPH-experiment 1.

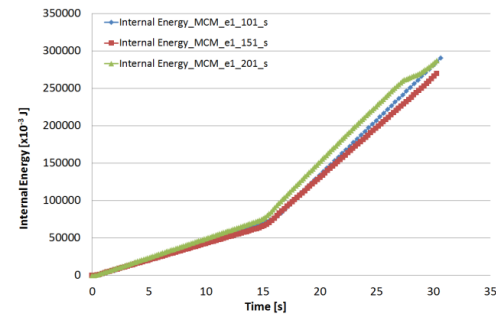


Figure 23 Internal energy for  $0 \leq t \leq 2 \cdot L/c$ ; SPH-experiment 1.

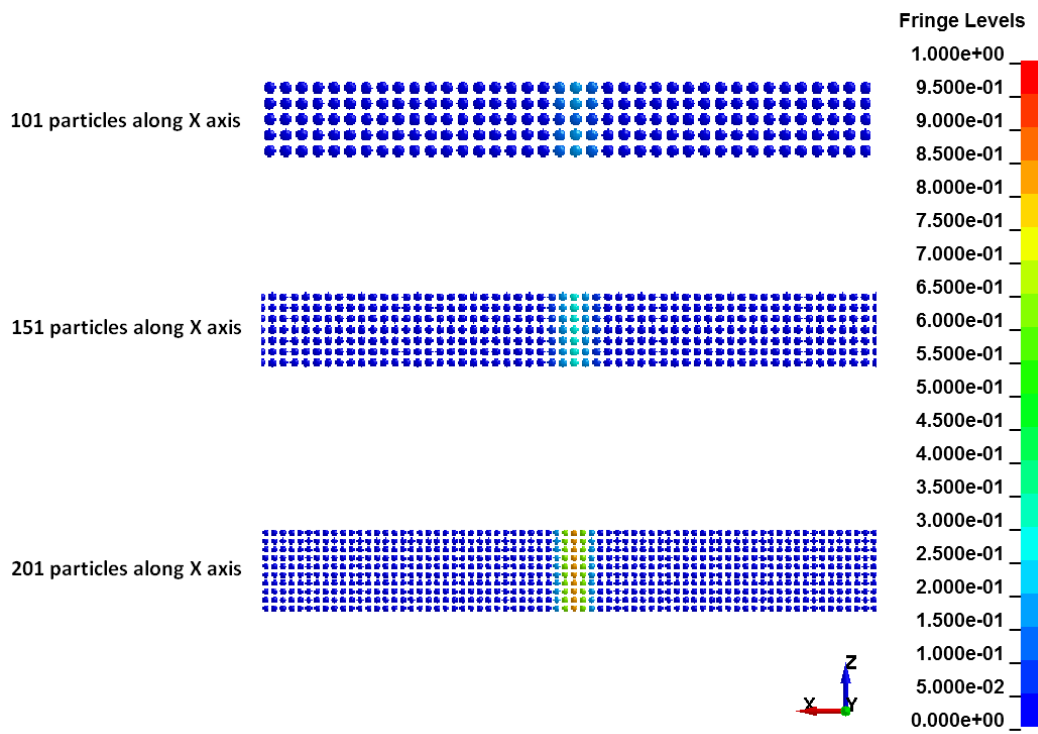


Figure 24 Localisation of damage within a limited area  $4h$  in size  $h=1.3 \cdot \Delta p$  around the bar symmetry plane at response time  $t=3/2 \cdot L/c_e$  (fringe level: damage [-]). SPH experiment 1

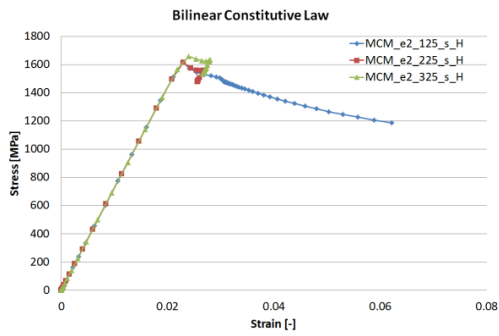


Figure 25 Longitudinal stress vs. longitudinal strain curves for the central particle obtained with different values of  $\lambda$ ; SPH-experiment 2

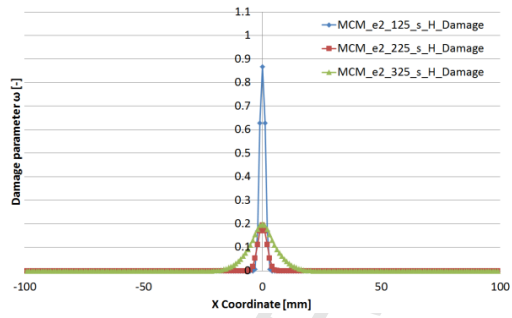


Figure 26 Damage distribution obtained with different values of smoothing lengths at response time  $t = 3/2 \cdot L/c_e$ ; SPH-experiment 2.

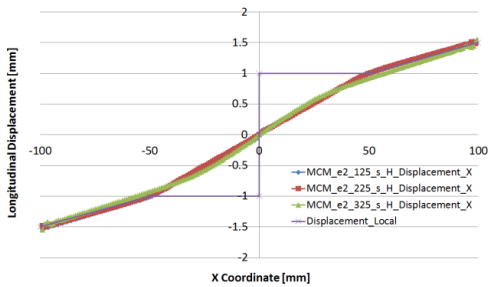


Figure 27 Analytical solution and the numerical results for longitudinal displacement at response time  $t = 3/2 \cdot L/c_e$ ; SPH-experiment 2.

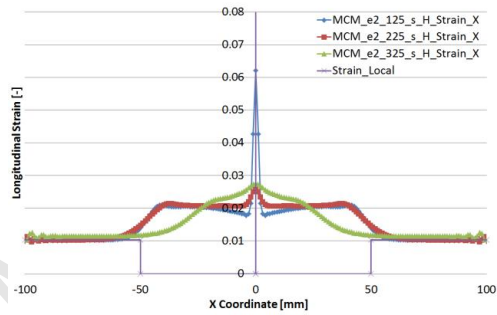


Figure 28 Analytical solution and the numerical results for longitudinal strain at response time  $t = 3/2 \cdot L/c_e$ ; SPH-experiment 2.

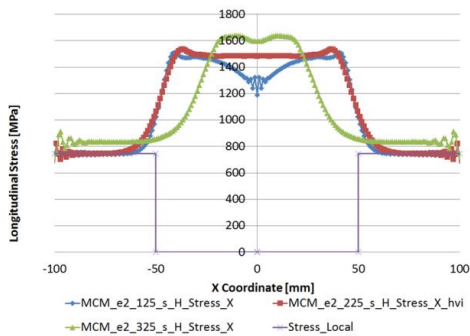


Figure 29 Analytical solution and the numerical results for longitudinal stress at response time  $t = 3/2 \cdot L/c_e$ ; SPH experiment 2.

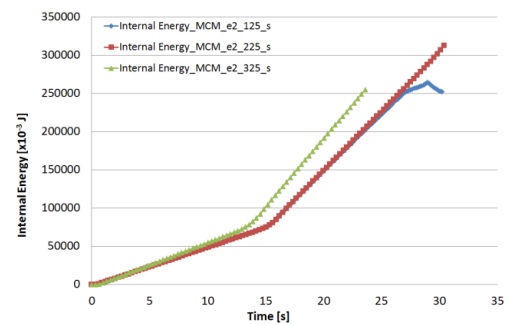


Figure 30 Internal energy for  $0 \leq t \leq 2 \cdot L/c$ ; SPH experiment 2.

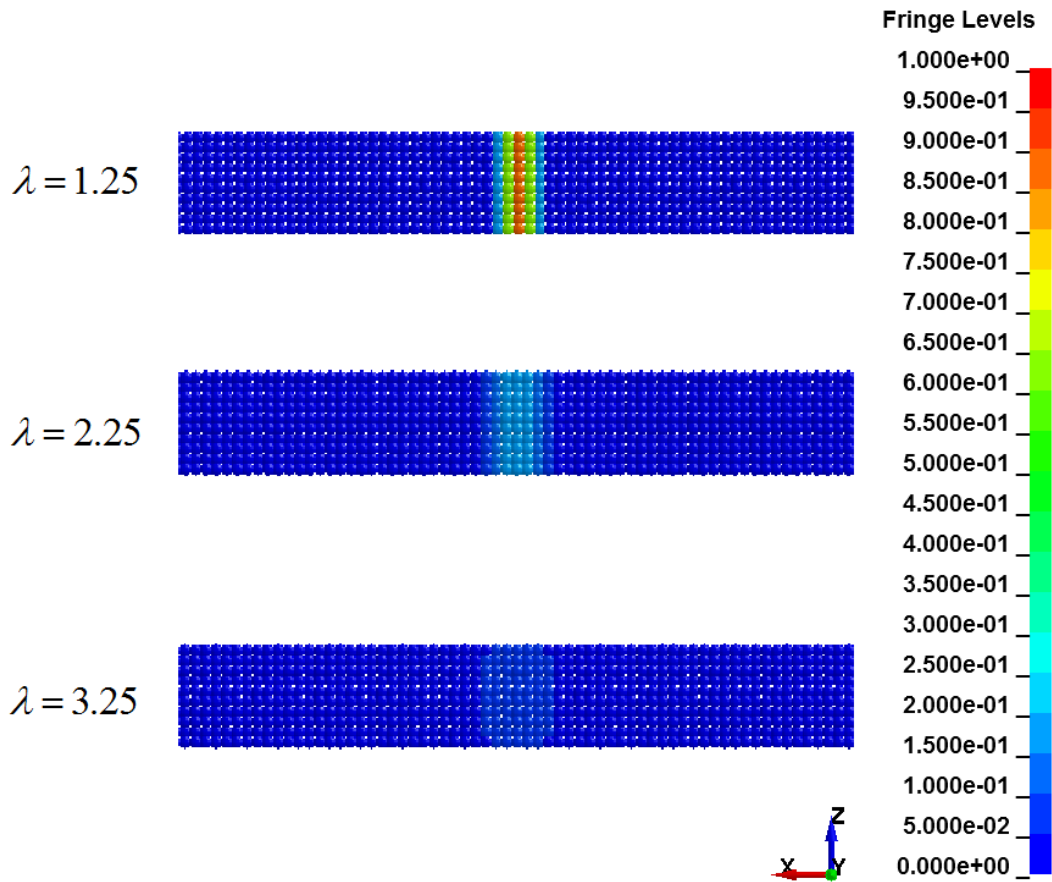


Figure 31 Localisation of damage within a limited area  $4h$  in size ( $h = \lambda \cdot 200\text{mm}/201$ ) around the bar symmetry plane at response time  $t = 3/2 \cdot L/c_e$  (fringe level plotted on the scaled particles for the sake of clarity: damage [-]); SPH experiment 2.

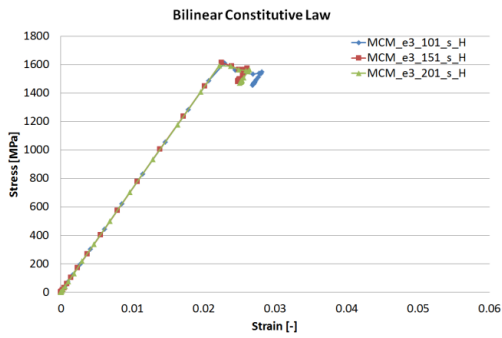


Figure 32 Longitudinal stress vs. longitudinal strain curves for the central particle obtained with different values of  $\Delta p$ ; SPH-experiment 3.

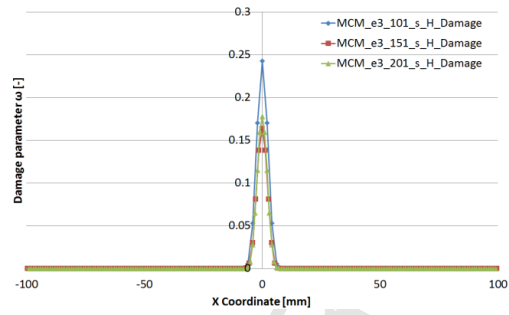


Figure 33 Damage distribution obtained with different particle densities at response time  $t = 3/2 \cdot L/c_e$ ; SPH-experiment 3.

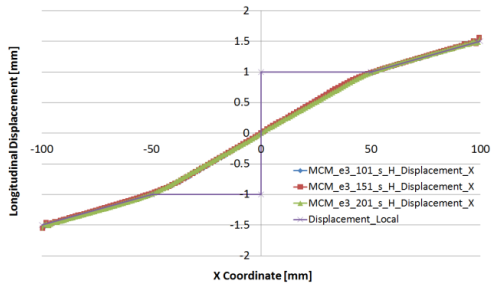


Figure 34 Analytical solution and the numerical results for longitudinal displacement at response time  $t = 3/2 \cdot L/c_e$ ; SPH-experiment 3.

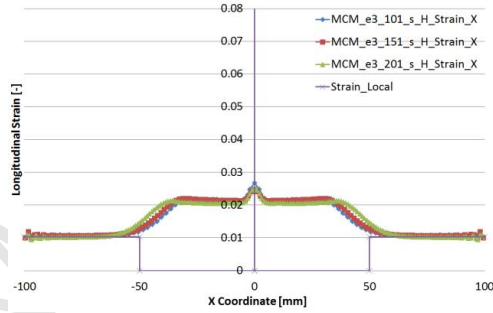


Figure 35 Analytical solution and the numerical results for longitudinal strain at response time  $t = 3/2 \cdot L/c_e$ ; SPH-experiment 3.

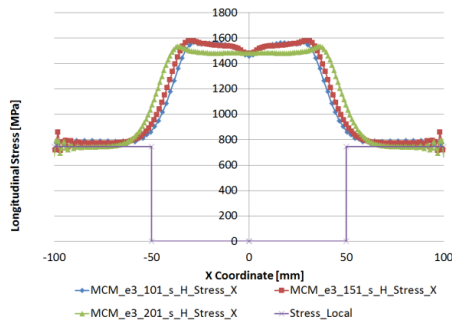


Figure 36 Analytical solution and the numerical results for longitudinal stress at response time  $t = 3/2 \cdot L/c_e$ ; SPH-experiment 3.

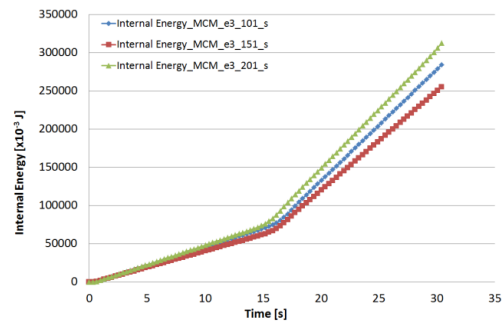


Figure 37 Internal energy for  $0 \leq t \leq 2 \cdot L/c$ ; SPH experiment 3.

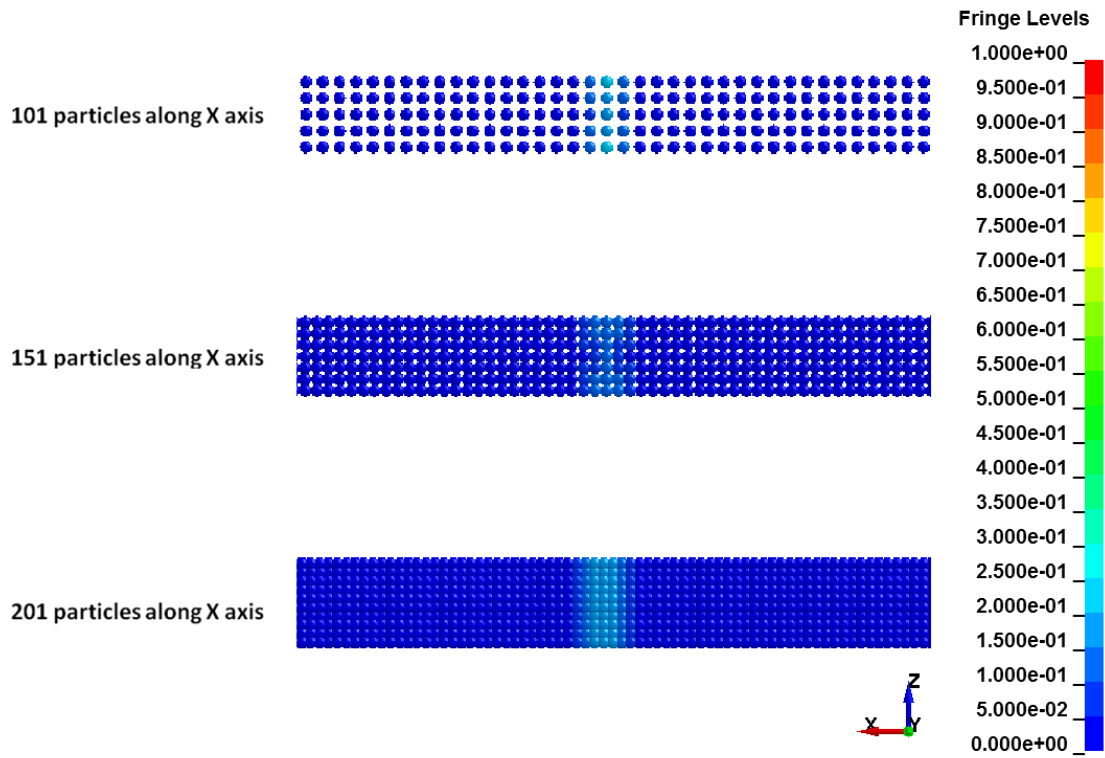


Figure 38 Localisation of damage within a limited area  $4h$  in size ( $h=2.5\text{mm}$ ) around the bar symmetry plane at response time  $t=3/2 \cdot L/c_e$  (fringe level: damage [-]); the damage distribution is independent of the interparticle distance  $\Delta p$ ; SPH experiment 3.

Table 3-1 Balance equations in continuum and SPH discrete forms Vignjevic et al. (2006)

Balance equations in continual and the SPH discrete forms		
mass	$\rho = J^{-1}\rho^0$	$\rho = J^{-1}\rho^0 = [\det\langle\mathbf{F}\rangle]^{-1}\rho^0$
momentum	$\rho^0\ddot{\mathbf{u}} = \nabla^0 \cdot \mathbf{P} + \mathbf{b}$	$\langle\ddot{\mathbf{u}}_i\rangle = -\sum_{j=1}^{mp} m_j \left( \frac{\mathbf{P}_i}{\rho_i^{02}} + \frac{\mathbf{P}_j}{\rho_j^{02}} \right) \nabla_{\mathbf{x}_i^0} W( \mathbf{x}_i^0 - \mathbf{x}_j^0 , h^0) + \mathbf{b}$
energy	$\rho^0\dot{e} = \mathbf{P} : \dot{\mathbf{F}}$	$\langle\dot{e}_i\rangle = \frac{\mathbf{P}_i}{\rho_i} : \sum_{j=1}^{mp} \frac{m_j}{\rho_j^0} (\mathbf{v}_i - \mathbf{v}_j) \otimes \nabla_{\mathbf{x}_i^0} W( \mathbf{x}_i^0 - \mathbf{x}_j^0 , h^0)$

Table 4-1: Input data for isotropic CDM model with linear strain-softening for FE (DYNA3D) and SPH (MCM)

Value	Sign	Magnitude	Unit
Density	$\rho$	$1.55 \cdot 10^{-9}$	<i>tonnes/mm<sup>3</sup></i>
Young's Modulus	$E$	70800	<i>MPa</i>
Poisson's ratio	$\nu$	0.125	—
Initial failure strain	$\varepsilon_i$	0.022	—
Critical failure strain	$\varepsilon_f$	0.060	—

Table 4-2: Summary of conditions for SPH Experiments 1, 2 and 3

Interparticle distance $\Delta p$ [mm]	Support domain factor $\lambda$ [-]	Physical smoothing length ( $h = \lambda \cdot \Delta p$ ) [mm]	Particles through thickness (y- and z- direction)	Particles along the length	Total number of particles
<b>Experiment 1: Influence of interparticle distance, <math>\Delta p = \text{variable}</math>, <math>\lambda = 1.3 = \text{constant}</math></b>					
200/101	1.3	260/101	5	101	2525
200/151		260/151	9	151	12231
200/201		260/201	11	201	24321
<b>Experiment 2: Influence of averaging over several neighbouring particles, <math>\Delta p = \text{constant}</math>, <math>\lambda = \text{variable}</math></b>					
200/201	1.25	250/201	11	201	24321
	2.25	150/67			
	3.25	650/201			
<b>Experiment 3: Influence of constant smoothing length, <math>\Delta p = \text{variable}</math>, <math>\lambda = \text{variable}</math>, <math>h = 25 \text{ mm}</math></b>					
200/101	1.2625	2.5	5	101	2525
200/151	1.8875		9	151	12231
200/201	2.5125		11	201	24321